2011

Crystallisation and Phase Transition Characteristics of Sol-Gel-Synthesized Zinc Titanates

Suresh Pillai
Dublin Institute of Technology, suresh.pillai@dit.ie

Michael Seery
Dublin Institute of Technology, michael.seery@dit.ie

Nicholas Nolan
Dublin Institute of Technology, nicholas.nolan@dit.ie

Recommended Citation

Nolan, N., Seery, M., Pillai, S.: Crystallisation and Phase Transition Characteristics of Sol-Gel-Synthesized Zinc Titanates. *Chemistry of mater* 2011, 23 (6), pp 1496–1504 doi:10.1021/cm1031688

2011-01-01

Crystallisation and Phase Transition Characteristics of Sol-Gel-Synthesized Zinc Titanates

Suresh C. Pillai

Michael Seery

Nicholas Nolan

The Crystallisation and Phase Transition Characteristics of Sol-gel Synthesised Zinc Titanates

Nicholas T. Nolan,[‡†] *Michael K. Seery,*[†] *and Suresh C. Pillai*[*‡]

School of Chemical and Pharmaceutical Sciences, Dublin Institute of Technology, Kevin Street, Dublin 8, Ireland and Centre for Research in Engineering Surface Technology (CREST), Focas Institute, Dublin Institute of Technology, Kevin Street, Dublin 8, Ireland

suresh.pillai@dit.ie

e-mail: suresh.pillai@dit.ie(SCP)

[‡] CREST, Dublin Institute of Technology.

[†] School of Chemical and Pharmaceutical Sciences, Dublin Institute of Technology.

Abstract

The synthesis of a ZnO-TiO_2 nanocomposite usually results in the formation of one or more of the three compounds such as Zn_2TiO_4, $Zn_2Ti_3O_8$ and $ZnTiO_3$ with other secondary impurity phases such as rutile-TiO_2 or ZnO. To obtain a phase-pure composite of either of these materials at a low processing temperature is one of the challenges in materials chemistry. For example, pure $ZnTiO_3$ can not be synthesised under normal conditions, because it transforms into Zn_2TiO_4 and rutile. $Zn_2Ti_3O_8$ is reported as a metastable form of $ZnTiO_3$. The Zn_2TiO_4 form is usually synthesized by a solid state reaction at high temperatures and typically above 1000 °C. In the current study, the crystalline and phase transformation behaviours of sol-gel synthesised zinc titanates has systematically been investigated with

regard to various Zn:Ti precursor molar ratios. X-ray diffraction has shown that with excess titanium precursor, zinc metatitanate ($ZnTiO_3$) is the preferred zinc titanate phase formed at temperatures 600 – 900 °C with direct transformation of zinc metatitanate to zinc orthotitanate (Zn_2TiO_4) occurring at 1000 °C. However, synthesis involving titanium precursor in the presence of excess zinc precursor forms $Zn_2Ti_3O_8$ with cubic defect spinel structure at temperatures 700 – 900 °C with direct transformation to zinc orthotitanate occurring at 1000 °C. The current study also indicated that the percentage of zinc titanate phases can be controlled by varying the initial sol-gel reaction conditions. Spectroscopic investigations have been carried out to understand the effect of precursor ($Zn(CH_3COO)_2.2H_2O$ and $H_2C_2O_4$) formulations on the crystallisation and phase transition behaviours of these composites. FTIR and Raman showed the presence of the oxalate form of zinc and titanium. However, either of these techniques could not reveal if the titanium oxalate chains exist separately from zinc oxalate chains or do they combine during the initial stages of preparation. A further powder x-ray diffraction investigation proposed that there were two separate metal oxalate chains formed during the synthesis. Additionally, it has previously been suggested that the formation of Zn_2TiO_4 and $Zn_2Ti_3O_8$ is limited by the presence of anatase and $ZnTiO_3$ only forms in the presence of rutile. Results from the present study confirm that in a sol-gel synthesis, the formation of various forms of zinc titanates is occurred by the presence of either anatase or rutile.

Introduction

Semiconductor research has shown great promise in recent times in areas such as hydrogen production through photocatalytic water splitting,[1] dye sensitized solar cells,[2] and photocatalytic remediation of harmful organics from air and water.[3, 4] Of the semiconductors investigated, titanium dioxide (TiO_2) has received the most attention due to its excellent stability, non-toxicity, cost and availability as well as its ability to produce highly oxidizing radicals.[5, 6] Zinc oxide (ZnO) has also shown promise in the areas of solar cells,[7] gas sensors[8, 9] and photocatalysis.[10]

The simultaneous synthesis of a ZnO/TiO_2 composite usually results in the formation of one or more of the three known compounds from the $ZnO\text{-}TiO_2$ system. They are Zn_2TiO_4 (zinc orthotitanate) with

cubic spinel crystal structure, $Zn_2Ti_3O_8$ with cubic defect spinel structure and $ZnTiO_3$ (zinc metatitanate) with rhombohedral ilmenite structure.[11-14] $Zn_2Ti_3O_8$ is the metastable, low temperature form of $ZnTiO_3$[14] but pure $ZnTiO_3$ is not easily obtained because it transforms into Zn_2TiO_4 and rutile.[12, 13]

Zinc orthotitanate (Zn_2TiO_4) is an inverse spinel that has been used as a catalyst and a pigment.[15] As a catalyst it is used as sorbent for the removal of sulfur from coal gasification product gases, in hot gas desulfurization units, at temperatures in the range 400 – 700 °C. Zinc orthotitanate can easily withstand these temperatures, but it is also one of the leading regenerable catalysts.[15-21] Zn_2TiO_4 may also be used for the photocatalytic splitting of water and the photocatalytic degradation of organic compounds.[22] Like other semiconductor photocatalyts, it has a wide band gap (3.1 eV) restricting its photocatalytic activity to UV light.[22, 23] It is usually synthesized by solid state reaction at high temperatures and typically, when a temperature below 1000 °C is used, longer heat treatments times are required.[15, 16, 18, 20, 24] Alternative synthesis methods have been employed such as the co-precipitation method. Heat treatment at 700 °C for 2 hours resulted in the formation of zinc orthotitanate, but secondary phases were also present.[17] A single phase material was obtained by Lew *et al* using the citrate method followed by heat treatment at 720 °C for 12 h.[19] Spinel type Zn_2TiO_4 was prepared by solid state reaction of ZnO and TiO_2 in molar ratios 3:2 at 1350 °C.[25, 26]

In the present study, a range of ratios of titanium and zinc precursors has been synthesised. The calcined powders were investigated by XRD and in order to investigate the molecular structure of the amorphous samples, FTIR and Raman spectroscopic techniques were employed. At optimum molar ratios, pure Zn_2TiO_4 was formed under low heating temperatures for short periods of time.

Experimental Section

Zinc acetate dehydrate (98 %), titanium tetraisopropoxide (TTIP, 97 %), oxalic acid (98.5 %) and acetic acid (AcOH, 99.7 %) were all purchased from Aldrich and used without further purification. Ethanol (99.5 %) was purchased from VWR international and used as received. Deionised water was used in all experimental techniques. In a typical synthesis, zinc acetate (9.17 g) was dissolved in ethanol (500 mL) at 60 °C. Oxalic acid dissolved in ethanol was then added slowly to the zinc acetate solution to

give a white, cloudy gel like suspension. To the resulting white cloudy suspension, TTIP (11.10 mL) was added, immediately followed by water (67.50 mL) This resulted in a molar ratio of Ti:Zn, 0.0375:0.05. The suspension was stirred for 2 hr before being aged in an oven in air at 100 °C for 48 hr to evaporate excess solvent. The resulting xerogel was then calcined at 400, 500, 600, 700, 800, 900 and 1000 °C for 2 hr at a ramp rate of 5 °C/min. The synthesis was repeated for six different molar ratios (table 1).

Table 1. Molar ratios and amounts of reactants used for synthesis of powders

Sample I.D.	Ti:Zn	ZnAcOH	EtOH	Oxalic	EtOH	TTIP	H_2O
TZ-4:1	0.05:0.0125	2.29 g	125 mL	3.15 g	50 mL	14.80 mL	90 mL
TZ-4:2	0.05:0.025	4.58 g	250 mL	6.30 g	100 mL	14.80 mL	90 mL
TZ-4:3	0.05:0.0375	6.88 g	375 mL	9.45 g	150 mL	14.80 mL	90 mL
TZ-1:4	0.0125:0.05	9.17 g	500 mL	12.60 g	200 mL	3.70 mL	22.50 mL
TZ-2:4	0.025:0.05	9.17 g	500 mL	12.60 g	200 mL	7.40 mL	45 mL
TZ-3:4	0.0375:0.05	9.17 g	500 mL	12.60 g	200 mL	11.10 mL	67.50 mL

A Siemens D 500 X-ray diffractometer, with a diffraction angle range 2Θ = 20 - 80° using Cu Kα radiation was used to collect XRD diffractograms. Quantitative phase analysis was estimated by comparing the integrated diffraction peaks from the different phases as described elsewhere.[27] Infrared spectra were recorded on a Perkin Elmer GX FTIR spectrometer and recorded as a KBr disc (1:10, sample/KBr). A Horiba Jobin Yvon LabRAM HR Raman system was used to obtain Raman spectra employing a laser excitation wavelength of 532 nm.

Results

X-ray Diffraction

Excess titanium precursor

The calculated phase compositions of samples TZ-4:1, TZ-4:2 and TZ-4:3 are shown in figure 1 (a–c). The phase compositions were calculated from the largest non-overlapping peaks of the representative phases from the X-ray diffractograms.

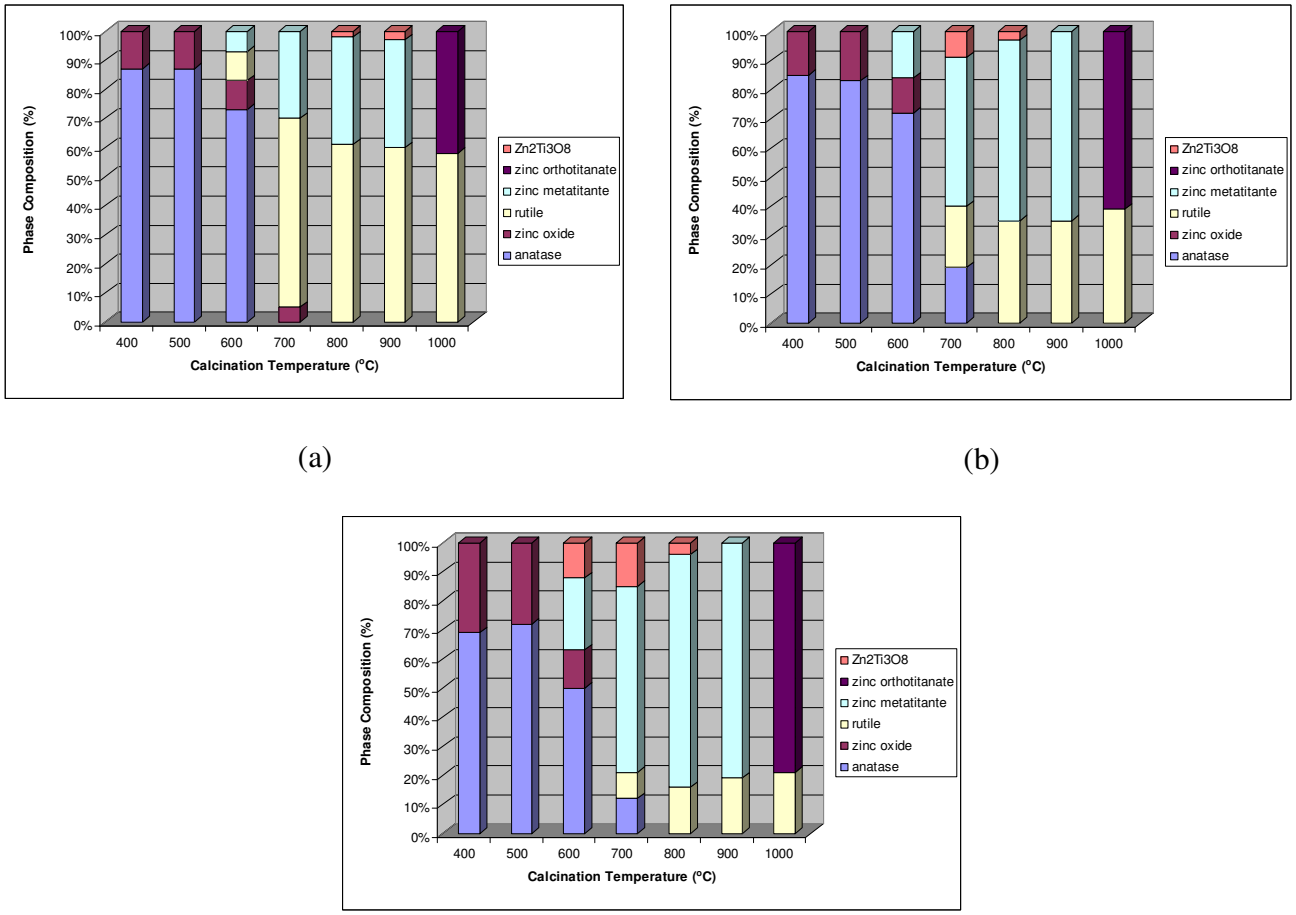

(a) (b)

(c)

Figure 1. Phase compositions of TZ-4:1 (a), TZ-4:2 (b) and TZ-4:3 (c)

Sample TZ-4:1 has the greatest excess of titanium precursor when compared with the other samples. This is clearly reflected in the composition of the phases. Anatase dominates at temperatures 400 – 600 °C and from 700 – 1000 °C rutile is the predominant phase. At calcination temperatures 400 and 500 °C, TiO_2 (87 %) and ZnO (13 %) exist separately. At 600 °C the metastable[28] zinc metatitante (7 %,

$ZnTiO_3$) begins to form, the crystallisation of zinc metatitante then accelerates as the temperature increases. At 700, 800 and 900 °C the sample is composed of 30 – 40 % zinc metatitante. Traces of the cubic spinel $Zn_2Ti_3O_8$ (2 – 3 %) can be found at 800 and 900 °C and at 1000 °C zinc orthotitante (42 %) and rutile are the only phases present.

As the amount of zinc precursor is increased (TZ-4:2 and TZ-4:3) the titania phase concentration is reduced and the amount of zinc titanates present increases as expected. As shown with TZ-4:1, TZ-4:2 at 400 and 500 °C are anatase (85 %) and zinc oxide only. As the temperature increases zinc titantes begin to form. It is interesting to note that at 600 °C, rutile is present for TZ-4:1, but rutile doesn't form until 700 °C for TZ-4:2 and TZ-4:3. Indicating that increased amounts of zinc precursor, delay the anatase to rutile transformation which is the opposite to that observed by Liu *et al*.[28] Samples TZ-4:2 and TZ-4:3 also contain anatase at 700 °C, TZ-4:1 does not, thus, providing further evidence that increased amounts of zinc precursor delay the anatase to rutile transformation. Increased amounts of zinc precursor also promote formation of the cubic spinel $Zn_2Ti_3O_8$ structure. For TZ-4:1, it forms at 800 °C (3 %), it is seen at 700 °C with TZ-4:2 (9 %) and it forms at 600 °C for TZ-4:3 (12 %). Also, as can be expected, at 1000 °C all samples consist of only zinc orthotitanate and rutile. As the amount of zinc precursor is increased, the amount zinc orthotitanate is also increased in an almost linear manner. For the samples calcined at 1000 °C, titanium:zinc ratios of 4:1 give 60/40 rutile/zinc orthotitante, ratios of 4:2 give 40/60 and a ratio of titanium:zinc 4:3 gives 80 % zinc orthotitante and 20 % rutile. A similar pattern is also observed for zinc metatitante but with other phases ($Zn_2Ti_3O_8$) also present. For all samples, the percentage of zinc metatitante at 800 and 900 °C was almost identical to the amount of zinc orthotitanate at 1000 °C indicating a direct transformation zinc metatitanate to zinc orthotitanate.

Infrared Spectroscopy

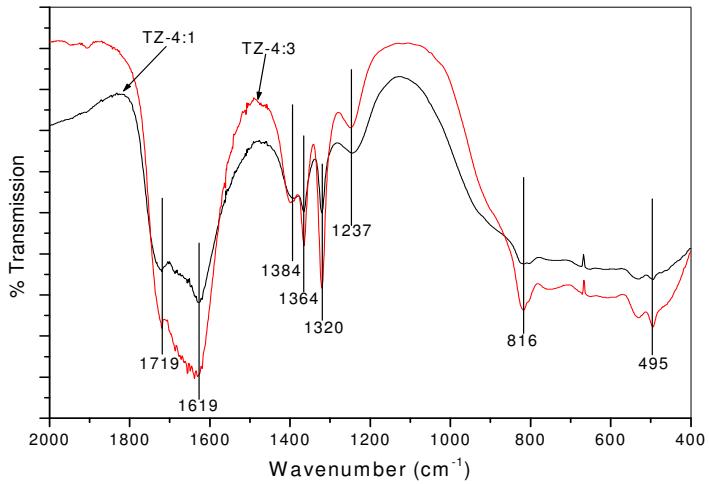

Figure 2. IR spectra of TZ-4:1 and TZ-4:3

Table 2. Assigned frequencies for IR spectra of TZ-4:1 and TZ-4:3.

Observed frequency (cm^{-1})	Assignments
1719	$\nu_{asym}(COO^-)$ titanium oxalate
1619	$\nu_{asym}(COO^-)$ zinc oxalate
1384	$\nu_{sym}(COO^-)$ titanium oxalate
1364	$\nu_{sym}(COO^-)$ zinc oxalate
1320	$\nu_{sym}(COO^-)$ zinc oxalate
1237	$\nu_{sym}(COO^-)$ titanium oxalate
816	δ_{asym}(O-C-O) zinc oxalate
495	ν(M-O) and δ_{asym}(C-C-O) zinc oxalate

Figure 2 shows the IR spectra of samples TZ-4:1 and TZ-4:3 before calcination. The assigned signals are summarized in table 2. The zinc oxalate signals are in agreement with Gabal *et al.*[29] Asymmetric (1719 cm^{-1}) and symmetric carboxylate stretches (1384 and 1237 cm^{-1}) are assigned to titanium oxalate. Comparing the IR spectra shown in figure 2 it can be seen that the presence of additional amounts of zinc cause an increase in the zinc oxalate $\nu_{asym}(COO^-)$ stretch at 1619 cm^{-1} relative to its titanium oxalate

equivalent at 1719 cm^{-1}. There is also an increase in the $\nu_{sym}(COO^-)$ stretches of zinc oxalate (1364 and 1320 cm^{-1}) compared to their titanium counterpart (1384 and 1237 cm^{-1}). These results are to be expected as an increase in zinc oxalate is going to provide an increase in the resulting peak intensities. The initial amounts of titanium and zinc will therefore control the composition of the metal oxalate chain. Any infrared features typical of Ti-OR coordination bonds[30] are not present in figure 2, suggesting that a polymeric zinc/titanium oxalate exists where OR groups have been removed.[30]

Raman Spectroscopy

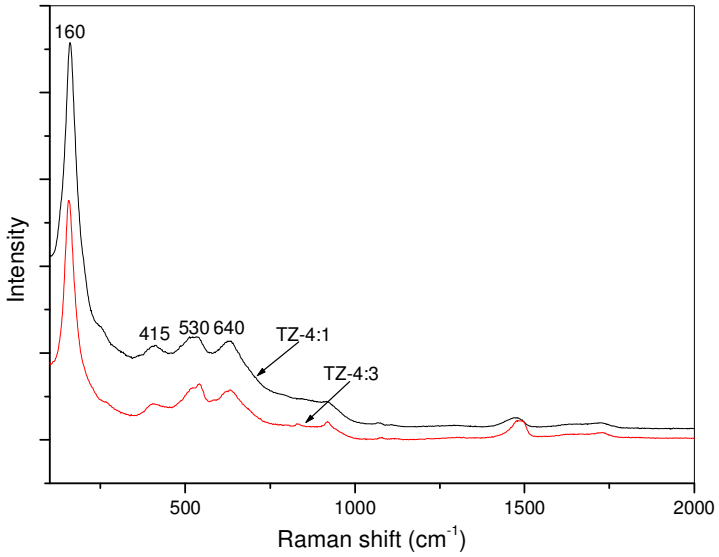

Figure 3. Raman spectra of TZ-4:1 and TZ-4:3

Figure 3 shows the Raman spectra of the samples TZ-4:1 and TZ-4:3 where titanium is in excess. The range 0 -1000 cm^{-1} represents the M-O stretches of the molecule. Peaks at 158, 418, 540 and 643 cm^{-1} are similar to those of the anatase four peak pattern.[31-33] It has been previously reported that during the crystallization process, titanium hydrolysate forms anatase/rutile like structures that can be detected by Raman. These Raman spectral patterns then disappear before the material crystallizes into anatase.[33] Raman studies show that Ti-O structures are dominating the metal oxide framework during the early processes of the reaction. This is expected as the titanium precursor is in excess over that of the zinc precursor. When the zinc precursor exceeds the titanium precursor, Raman spectra with different spectral profiles are obtained.

Excess Zinc Precursor

XRD

The x-ray diffractogram of TZ-1:4 (figure 4) shows that ZnO is the only crystal structure present at temperatures 400 and 500 °C. Zinc orthotitanate begins to form at 600 °C, and from 700 – 1000 °C, zinc orthotitanate and zinc oxide peak intensity grows stronger, indicating an increase in crystallinity for both phases. There are no TiO_2 phases present at any temperature.

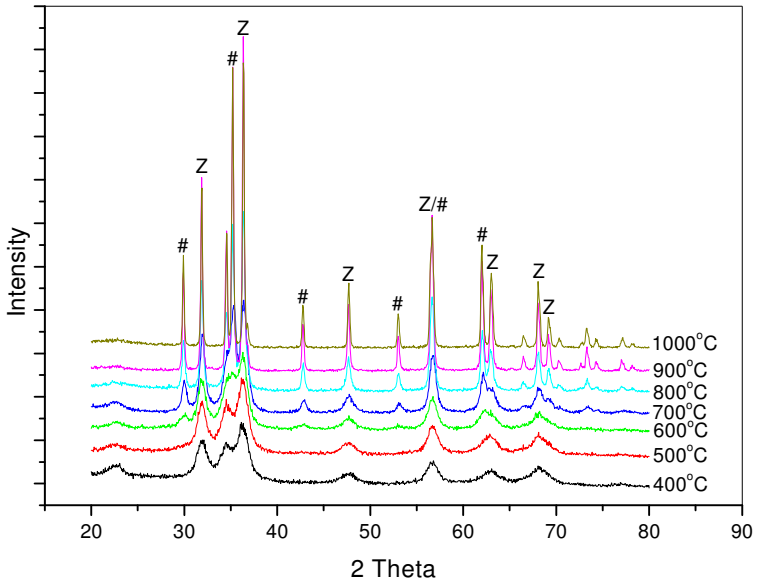

Figure 4. XRD of TZ-1:4, Z-ZnO and #-$TiZn_2O_4$

As the titanium precursor was increased, TZ-3:4, anatase is present along with zinc oxide at calcination temperatures 400 and 500 °C (figure 5). At 600 and 700 °C the metastable $Zn_2Ti_3O_8$ is the only phase present. At 800 °C zinc metatitanate forms along with $Zn_2Ti_3O_8$ and at 900 °C the sample consists of zinc metatitante and either $Zn_2Ti_3O_8$ or zinc orthotitanate. At 1000 °C zinc orthotitanate is the dominant phase with trace amounts (3%) of rutile present.

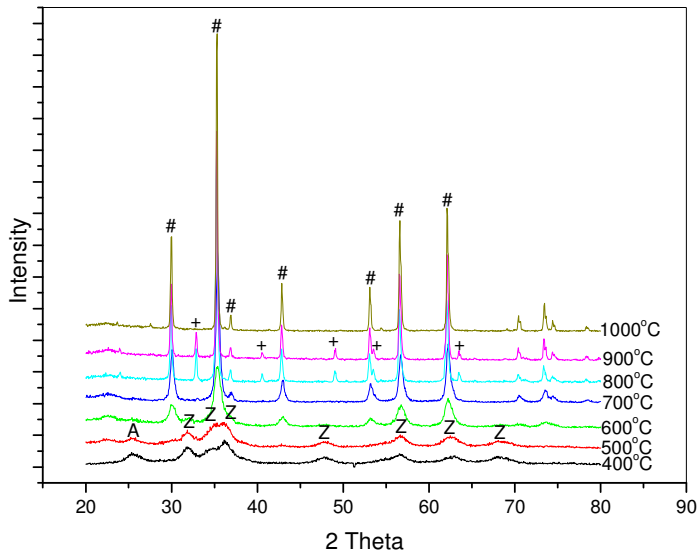

Figure 5. XRD of TZ-3:4, R-rutile, Z-ZnO, +-$ZnTiO_3$ and #-$TiZn_2O_4$

Figure 6 (a-c) summarises the compositions for samples TZ-1:4, TZ-2:4 and TZ-3:4. For lower calcination temperatures the primary zinc oxide peak was overlapping with $Zn_2Ti_3O_8$ (and zinc orthotitanate) peak and as such the composition percentages could not be determined at temperatures 400 – 600 °C. However, from the XRD diffractograms (figure 4 and 5) it can be seen that zinc oxide is the only phase present at temperatures 400 and 500 °C for TZ-1:4 (figure 4) and the same was seen for TZ-2:4, however, figure 5 (TZ-3:4) shows that both anatase and zinc oxide are present at 400 and 500 °C, while at 600 and 700 °C the only the metastable $Zn_2Ti_3O_8$ exists. From figure 6 (a-c), it is clear that the amount of $Zn_2Ti_3O_8$ increases with increasing amounts of titanium precursor at temperatures 700 – 900 °C. The same trend is also noticed for zinc orthotitanate. Results infer that $Zn_2Ti_3O_8$ directly transforms into zinc orthotitanate without affecting the zinc oxide crystal as can be seen for samples TZ-1:4 and TZ-2:4 (figure 6 a & b). Results for sample TZ-3:4 (figure 6, c) indicate the same direct $Zn_2Ti_3O_8$ to zinc orthotitanate transformation with the minor phase, zinc metatitanate transforming to rutile.

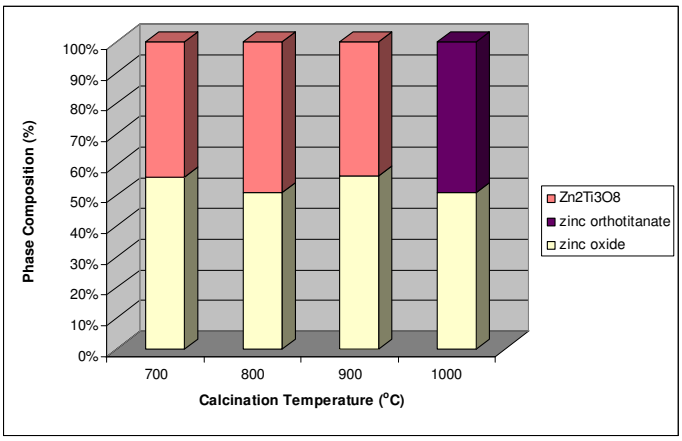

(a)

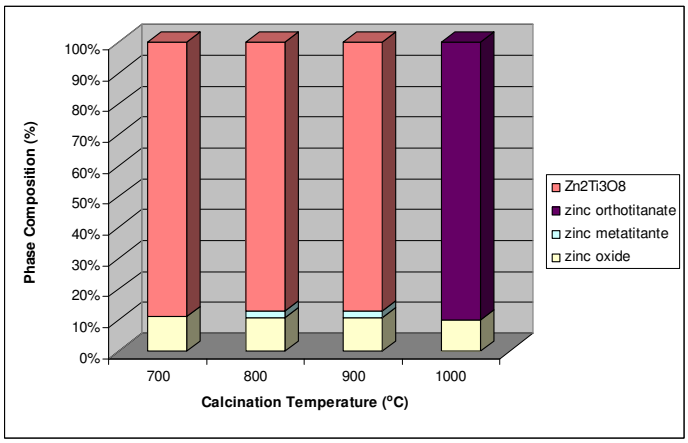

(b)

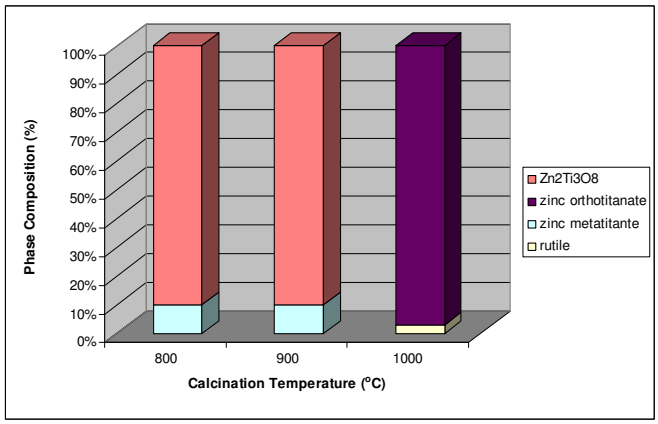

(c)

Figure 6. Phase composition of (a)TZ-1:4, (b) TZ-2:4 and (c) TZ-3:4

The results show that near identical amounts of $Zn_2Ti_3O_8$ transform to zinc orthotitanate when zinc precursor is in excess over titanium, this behaviour is adherently different to the excess titanium system where results showed that zinc metatitanate transformed to zinc orthotitanate. Since this synthesis is not a typical solid state reaction but a sol-gel reaction of titanium and zinc precursors, it is necessary to understand if the amorphous metal oxide structure influences the final crystalline structure. To determine what is happening with the metal oxide system in the early stages of the reaction, FTIR and Raman spectroscopic techniques were carried out on the samples before calcination to determine the structure of the amorphous metal-oxide frameworks.

Infrared Spectroscopy

When excess titanium is present XRD has shown that at low calcination temperatures (400 – 600 °C) anatase TiO_2 is favoured over zinc oxide and at higher temperatures (700 – 1000 °C) rutile TiO_2 dominates while zinc metatitanate transforms into zinc orthotitanate between 900 and 1000 °C.

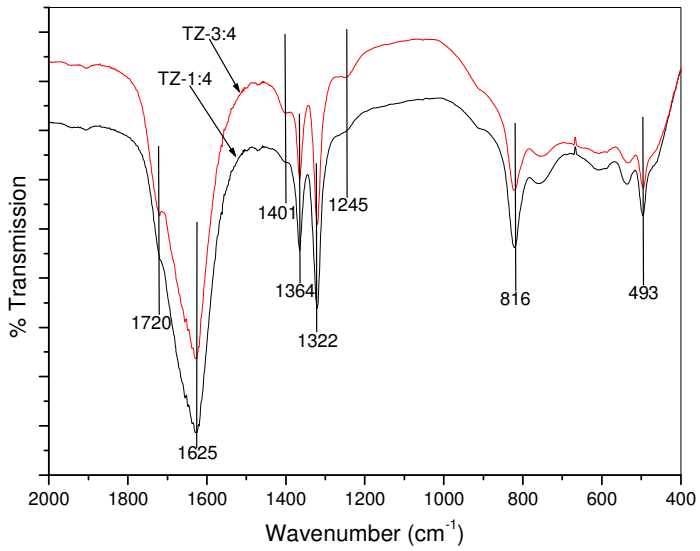

Figure 7. IR spectra of TZ-1:4 and TZ-3:4

The IR spectra of samples TZ-1:4 and TZ-3:4 are shown in figure 7. For TZ-1:4 peaks at 1720 and 1401, 1245 cm^{-1} which represent COO^-_{asym} and COO^-_{sym} of titanium oxalate respectively are significantly decreased when compared with the spectra of TZ-4:1 (figure 2). However, as the titanium ratio increases (TZ-3:4), peaks at 1720, 1401 and 1245 cm^{-1} appear, indicating the presence of titanium oxalate in the metal oxalate chain. Peaks at 816 and 493 cm^{-1} representing δ_{asym}(O-C-O) and ν(M-O), δ_{asym}(C-C-O) respectively are more intense for sample TZ-1:4 than for TZ-3:4. Again this shows that with greater amounts of zinc precursor, zinc oxalate dominates the metal oxalate chain network.

Symmetric and asymmetric carboxylate stretches from titanium and zinc oxalate are clearly present in shown IR spectra. As expected when the zinc precursor is in excess, carboxylate stretches of titanium oxalate are weak. However, when titanium is in excess, strong signals representative of zinc oxalate are still clear. This can be explained through the synthesis where zinc acetate is first reacted with oxalic acid

to give zinc oxalate before titanium isopropoxide is added. Therefore, TTIP can chelate with unreacted oxalic acid.

Raman Spectroscopy

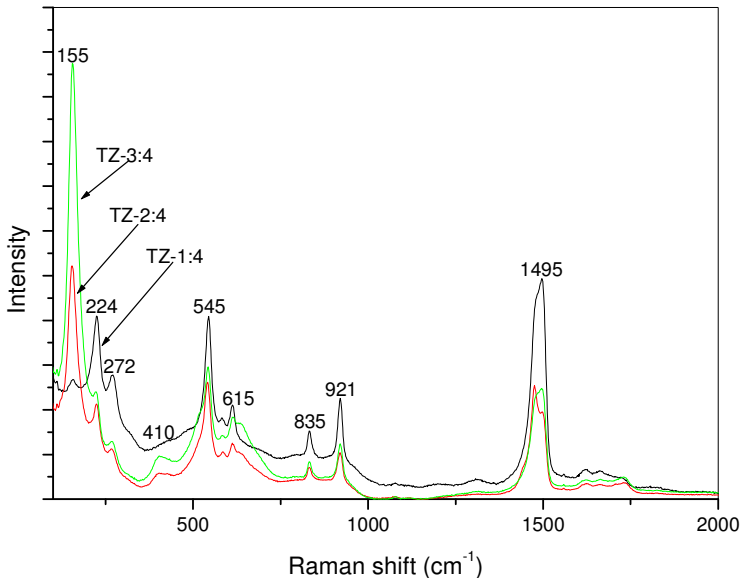

Figure 8. Raman spectra of TZ-1:4, TZ-2:4 and TZ-3:4

The Raman spectra of excess zinc samples TZ-1:4, TZ-2:4 and TZ-3:4 is shown in figure 8. Peaks representative of the anatase four peak pattern[31-33] are present at 155, 415, 545 and 615 cm^{-1}. All other signals in the region 0 – 1000 cm^{-1} are believed to be caused by Zn-O contributions. There is a large signal at 1495 cm^{-1} due to $(COO^{-})_{sym}$ stretching of the oxalate group. Comparing peak intensities of 1495 cm^{-1} with M-O peaks it is clear that this signal is largest relative to its surrounding peaks for TZ-1:4 and as the titanium ratio increases, the carboxylate peak decreases. Again, this is evidence of the dominant effect of zinc oxalate in the metal oxalate chain. The Raman spectra of TZ-2:4 and TZ-3:4 give similar peak positions to each other but comparison on of the profile of TZ-1:4, it can be seen that TZ-1:4 gives a spectrum that contains no similarities with either TZ-2:4 and TZ-3:4. In the spectra of TZ-2:4 and TZ-3:4 the increased levels of titanium lead to signals at 155, 415, 545 and 615 cm^{-1}, but the spectrum of TZ-1:4 does display these peaks. It was therefore speculated that all peaks shown in the spectrum of TZ-1:4 (figure 8) arise from Zn-O stretches.

The presence of the highlighted peaks show the dominant influence of the titanium as the ratio is increased. Comparison of figure 3 with figure 8 also shows that Ti-O bonds give exceptionally higher Raman signals than Zn-O. It can also be shown upon comparison of both IR and Raman spectra that there is no coincidence between the peak profile of either. This suggests that the rule of mutual exclusion may be applied to the titanium-zinc oxalate structures.[34] Applying the rule of mutual exclusion would give a centrosymmetric structure, where the metal atoms occupy a position equidistant from the coordinating oxygens.[34] Summarising the spectroscopic results it can be shown that:

- Oxalic acid chelates to titanium to form titanium oxalate
- Increasing zinc oxalate causes reduction in asymmetric and symmetric carboxylate stretches from titanium oxalate and an increase in the symmetric stretch in Raman
- When Ti is in excess, the anatase four peak pattern dominates the Raman spectra and there is a broad signal without significant individual peak contributions in IR (400 – 1000 cm^{-1})
- When Zn is in excess, the four peak pattern is reduced in Raman and the IR spectra show individual peaks representative of O-C-O and M-O from zinc oxalate
- There is a metal oxalate chain composed of titanium and zinc
- In IR, asymmetric and symmetric carboxylate stretches for zinc oxalate are always present, but carboxylate stretches are only present for titanium oxalate at high ratios
- The rule of mutual exclusion can be applied, indicating the presence of a symmetric molecule

Discussion

Ishioka *et al* showed the structure of zinc acetate dihydrate (figure 9) through X-ray crystallography.[35]

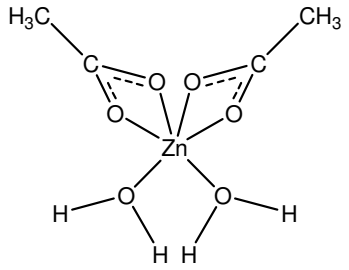

Figure 9. Molecular structure of zinc acetate dihydrate.

Reacting oxalic acid with zinc acetate forms the intermediate zinc oxalate (scheme 1) as presented by Kanade *et al*.[36]

$$Zn(CH_3COO)_2.2H_2O + H_2C_2O_4 \rightarrow ZnC_2O_4.2H_2O + 2AcOH + 2H_2O \qquad \text{(Scheme 1)}$$

X-ray crystallographic studies of zinc oxalate show that zinc is octahedrally coordinated to six oxygen atoms[37, 38] as shown in figure 10a. It is also been shown that divalent metal cations and oxalate groups generate an infinite chain arrangement as depicted in figure 10b.[39, 40]

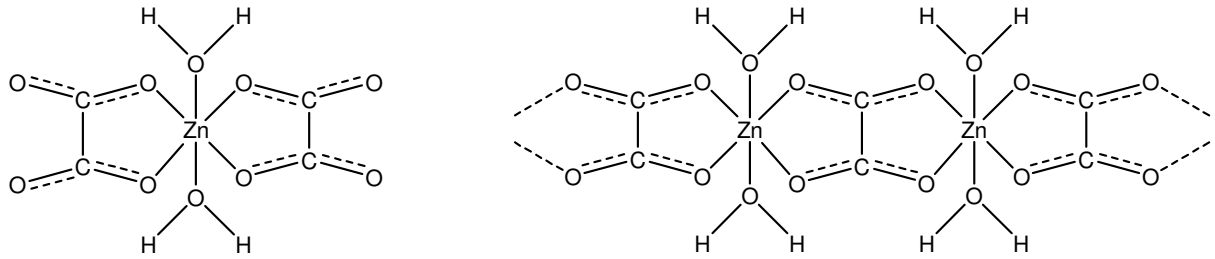

Figure 10. Molecular structure of zinc oxalate dihydrate (a) and the infinite chain arrangement (b).

Thermal treatment of zinc oxalate leads to the formation of zinc oxide. TGA/DTA studies have shown the removal of water at 120 °C and the decomposition of zinc oxalate at 400 °C as shown in scheme 2.[36]

$$ZnC_2O_4.2H_2O + \tfrac{1}{2}O_2 \rightarrow ZnO + 2CO_2 + 2H_2O \qquad \text{(Scheme 2)}$$

The system under investigation in this study is not zinc oxalate alone but it also includes varying ratios of titanium isopropoxide (figure 11a) which consists of monomeric units.[41] It has been previously reported that acetic acid,[42, 43] formic acid[44] and acetyl acetone[45] chelate to titanium isopropoxide. As was

shown with zinc oxalate,[39, 40] titanium isopropoxide also forms chains upon reaction with a chelating agent figure 11b.[46-48]

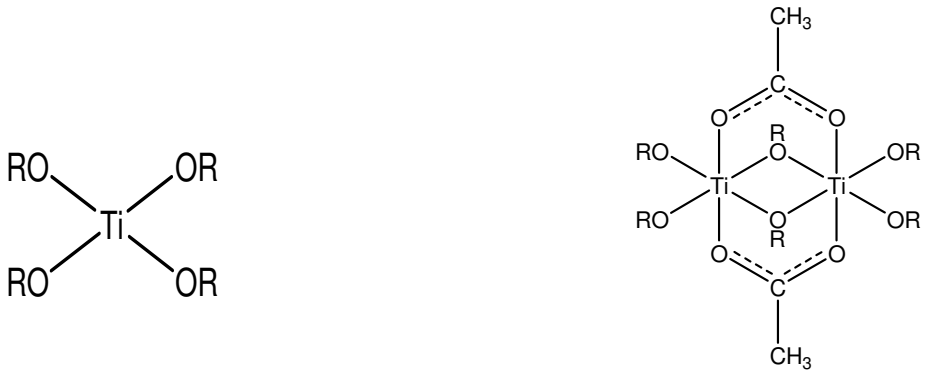

(a) (b)

Figure 11. Molecular structure of titanium isopropoxide a) before chelation and b) after chelation.

During the sol gel reaction of titanium alkoxides, the OR groups are preferentially hydrolysed while the ligands remain tightly bound throughout much of the condensation process. Thus promoting the formation of linear chains of Ti-O polymers composed of edge sharing octahedra.[43, 49] The formation of these octahedral stabilises TiO_2 as anatase thus lowering the anatase to rutile transformation temperature.[43, 49]

Previous research has shown the structure of zinc oxalate[37, 38] and titanium carboxylates.[42-44] From the results shown through IR and Raman it is known that titanium and zinc oxalate are present (figure 12), but it can not be shown if titanium oxalate chains exist separately from zinc oxalate chains or do they combine. X-ray diffraction results showed that initially crystalline ZnO or TiO_2 anatase formed separately and at higher calcination temperatures, zinc titanates were formed. This indicates that there were two separate metal oxalate chains formed during the synthesis (figure 12 a & b).

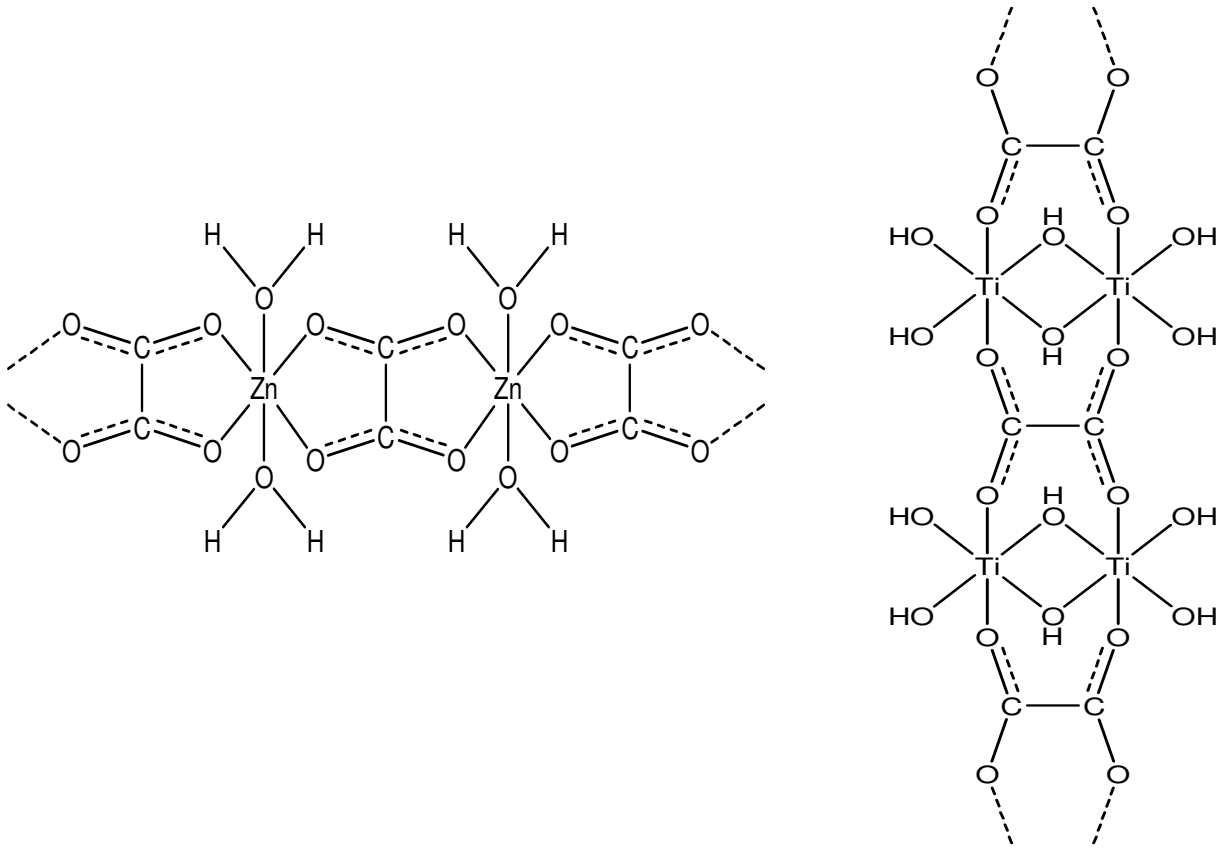

(a) (b)

Figure 12. Proposed structures of metal oxalate chains formed a) zinc and b) titanium

As the condensation process proceeds with excess titanium (TZ-4:1), TiO_6 octahedra form TiO_2 anatase and ZnO_4 tetrahedra form ZnO (wurtzite). As the calcination temperature becomes more intense (≥ 600 °C), the TiO_6 octahedra and ZnO_4 tetrahedra undergo molecular rearrangement and phase transformation occurs. Zinc oxide tetrahedral and TiO_6 octahedra undergo further movement and combine to form zinc titanates and rutile. The metastable zinc metatitanate and stable rutile exist at 800 and 900 °C with trace amounts of $Zn_2Ti_3O_8$ also present. At 1000 °C zinc metatitanate and $Zn_2Ti_3O_8$ decompose to form zinc orthotitanate, rutile remains the dominant phase. As the amount of zinc precursor increases (TZ-4:2 and TZ-4:3), the crystals behave in a similar manner but with increasing amounts of zinc oxide at early calcination temperatures (400 and 500 °C) and greater amounts of zinc titanates at temperatures ≥ 700 °C. It is clear from the results (figure 1 a-c), that the percentage of zinc titanate at 700 °C is very similar to the final percentage of zinc orthotitanate. The results have shown

that at temperatures 700 – 900 °C for samples with excess titanium precursor, zinc metatitante is the dominant zinc titanate phase and is stable up to 900 °C, it then undergoes complete transformation to form zinc orthotitanate. Phase transformation is almost 100 % zinc metatitante to zinc orthotitanate, however, results do show that rutile is also formed. Calculated values for percentage conversion are 90 % for TZ-4:1, 93 % for TZ-4:2 and 98 % for TZ-4:3 reflecting an increase in conversion in line with increasing zinc precursor ratio.

Three different molar ratios where zinc precursors are in excess over titanium were also prepared. All three behaved differently to those where titanium was in excess. For all samples where zinc is in excess, accurate compositions at calcination temperatures 400 – 600 °C could not be obtained from the X-ray diffractograms as the peaks were not resolved but from the diffractograms it was clear that zinc oxide was the dominant phase at early temperatures with anatase also present in small amounts. However, the percentage composition was calculated from results of temperatures 700 °C onwards (figure 6 a -c). When titanium was in excess a clear transformation of large compositions of zinc metatitanate to zinc orthotitanate was noticed. With excess zinc, zinc metatitanate is not present in TZ-1:4, for TZ-2:4, trace amounts of zinc metatitanate (2%) are present at 800 and 900 °C and as the titanium ratio increases (TZ-3:4), larger amounts of zinc metatitanate (10%) are present at calcination temperatures 800 and 900 °C. With excess zinc, $Zn_2Ti_3O_8$ was the dominant, metastable phase formed at temperatures 700 – 900 °C, total phase transformation occurred at temperatures > 900 °C and zinc orthotitanate was formed. Unlike the excess titanium system where zinc metatitanate transformed to zinc orthotitanate and rutile with conversion percentages of between 90 – 98 %, when zinc was in excess it was $Zn_2Ti_3O_8$ combining with zinc oxide transforming into zinc orthotitanate. Conversion percentages of $Zn_2Ti_3O_8$ of greater than 100 % were calculated for TZ-1:4 (104 %), TZ-2:4 (101 %) and TZ-3:4 (107 %), values greater than 100 % are achieved because unlike zinc metatitanate that transforms to zinc orthotitanate and rutile, it appears that when zinc precursor is used in excess, $Zn_2Ti_3O_8$ is the favoured phase and it combines with zinc oxide to form zinc metatitanate.

The structures of all zinc titanates studied here share common features; they all consist of TiO_6 octahedra that are connected over common edges.[28] Anatase displays similarities with the spinel structures of Zn_2TiO_4 and $Zn_2Ti_3O_8$ but $ZnTiO_3$ shares its structure with rutile.[28, 50] As such, it has previously been suggested that the formation of Zn_2TiO_4 and $Zn_2Ti_3O_8$ is limited by the presence of anatase and $ZnTiO_3$ only forms in the presence of rutile.[11, 51] However, subsequent researchers have shown that this is not necessarily the case.[27, 28, 51] Results from the present study show that for samples where titanium is in excess (TZ-4:1, TZ-4:2 and TZ-4:3) anatase and zinc oxide are present during the early stages of crystallisation (400 – 600 °C) and as the calcination temperature increases, zinc metatitanate is formed, greater amounts of metatitanate are formed with an increased percentage of zinc oxide. These results suggest that in a sol-gel synthesis, the formation of zinc metatitanate is determined by not only the presence of titanium dioxide (anatase or rutile) but also on the presence of zinc oxide. With excess zinc precursor (TZ-1:4, TZ-2:4 and TZ-3:4), zinc oxide was the dominant crystalline phase for calcination temperatures 400 – 600 °C and as the temperature increased, $Zn_2Ti_3O_8$ became the dominant phase, transforming to zinc orthotitanate at 1000 °C. Again this result shows that anatase is not necessary for the formation of $Zn_2Ti_3O_8$ and that the percentage of zinc oxide influences what zinc titanate phase is formed.

Conclusions

A series of zinc titanate powders was successfully synthesised using a simple sol-gel technique. The effect of varying ratios of zinc/titanium precursors was investigated. The powders were calcined at temperatures ranging from 400 – 1000 °C and the crystalline phases of the powders were determined using X-ray diffraction.

To determine the molecular structures of the samples before they underwent calcination, infrared and Raman spectroscopy were employed. Possible structures of zinc oxalate and titanium oxalate were proposed, based on spectroscopic results obtained and from what is known from the literature. It was suggested that both the titanium oxalate and the zinc oxalate remain separate throughout the reaction which may be shown through XRD results of the powders calcined at low temperatures.

It was shown that low percentages of zinc oxide result in the formation of the metastable zinc metatitanate which ultimately transforms (90 – 98 % conversion) to zinc orthotitanate (< 900 °C) with rutile from 700 °C onwards. When zinc oxide is the dominant structure during the early stages of crystallisation (400 and 500 °C), $Zn_2Ti_3O_8$ is the zinc titanate phase preferentially formed as the calcination temperature increases. It transforms to zinc orthotitanate at 1000 °C.

References

1. Fujishima, A.; Honda, K., *Nature* **1972,** 238.
2. O'Regan, B.; Gratzel, M., *Nature* **1991,** 353, 737 - 740.
3. Fox, M. A.; Dulay, M. T., *Chem. Rev.* **1993,** 93, 341 - 357.
4. Hoffmann, M. R.; Martin, S. T.; Choi, W.; Bahnemann, D. W., *Chem. Rev.* **1995,** 95, 69 - 96.
5. Kuo, Y.-L.; Chen, H.-W.; Ku, Y., *Thin Solid Films* **2007,** 515, 3461 - 3468.
6. Yu, J.; Yu, H.; Ao, C. H.; Lee, S. C.; Yu, J. C.; Ho, W., *Thin Solid Films* **2006,** 496, 273 - 280.
7. Kluth, O.; Schope, G.; Hupkes, J.; Agashe, C.; Muller, J.; Rech, B., *Thin Solid Films* **2003,** 442.
8. Choi, W. S.; Kim, E. J.; Seong, S. G.; Kim, Y. S.; Park, C.; Hahn, S. H., *Vacuum* **2009,** 83, 878 - 882.
9. Zhang, Q.; Zhang, S.; Xie, C.; Fan, C.; Bai, Z., *Sens Actuators B* **2008,** 128.
10. Georgekutty, R.; Seery, M. K.; Pillai, S. C., *J. Phys. Chem. C.* **2008,** 112, 13563 - 13570.
11. Bartram, S. F.; Slepetys, R. A., *J. Am. Ceram. Soc.* **1961,** 44, 493 - 499.
12. Dulin, F. H.; Rase, D. E., *J. Am. Ceram. Soc.* **1960,** 43, 125 - 131.
13. Mohammadi, M. R.; Fray, D. J., *ECERS* **2010,** 30, 947 - 961.
14. Yamaguchi, O.; Morimi, M.; Kawabata, H.; Shimizu, K., *J. Am. Ceram. Soc.* **1987,** 70, C97 - C98.
15. Chaves, A. C.; Lima, S. J. G.; Araujo, R. C. M. U.; Maurera, M. A. M. A.; Longo, E.; Pizani, P. S.; Simoes, L. G. P.; Soledade, L. E. B.; Souza, A. G.; dos Santos, I. M. G., *J. Solid State Chem.* **2006,** 179, 985 - 992.
16. Alonso, L.; Palacios, J. M.; Moliner, R., *Energy Fuel* **2001,** 15, 1396 - 1402.
17. Jothimurugesan, K.; Gangwal, S. K., *Ind. Eng. Chem. Res.* **1998,** 37, 1929 - 1933.
18. Jun, H. K.; Lee, T. J.; Ryu, S. O.; Kim, J. C., *Ind. Eng. Chem. Res.* **2001,** 40, 3547 - 3556.
19. Lew, S.; Sarofim, A. F.; Flytzani-Stephanipoulos, M., *Chem. Eng. Sci.* **1992,** 47, 1421 - 1431.
20. Pineda, M.; Fierro, J. L. G.; Palacios, J. M.; Cilleruelo, C.; Garcia, E.; Ibarra, J. V., *Appl. Surf. Sci.* **1997,** 119, 1 - 10.
21. Slimane, R. B.; Abbasian, J., *Adv. Environ. Res.* **2000,** 4, 147 - 162.
22. Jang, J. S.; Borse, P. H.; Lee, J. S.; Lim, K. T.; Jung, O.-S.; Jeoung, E. D.; Bae, J. S.; Won, M. S.; Kim, H. G., *Bull. Korean Chem. Soc.* **2009,** 30, 3021 - 3024
23. Matsumoto, Y., *J. Solid State Chem.* **1996,** 126.
24. Kim, H. T.; Byun, J. D.; Kim, Y. S., *Mater. Res. Bull.* **1998,** 34, 963 - 973.
25. Li, C.; Bando, M.; Nakamura, M.; Kimizuka, N.; Kito, H., *Mater. Res. Bull.* **2000,** 35, 351 - 358.
26. Sedpho, S.; Wongratanaphisan, D.; Mangkorntong, P.; Mangkorntong, N.; Choopun, S., *J. Nat. Sci.* **2008,** 7, 99 - 104.
27. Yang, J.; Swisher, J. H., *Mater. Charac.* **1996,** 37, 153 - 159.
28. Liu, Z.; Dongxiang, Z.; Gong, S.; Li, H., *J. Alloys Compd.* **2009,** 475, 840 - 845.
29. Gabal, M. A.; El-Bellihi, A. A.; El-Bahnasaway, H. H., *Mater. Chem. Phys.* **2003,** 81, 174 - 182.
30. Doeuff, S.; Henry, M.; Sanchez, C.; Livage, J., *J. Non-Cryst. Solids* **1987,** 89, 206 - 216.

31. Hwang, D. S.; Lee, N. H.; Lee, D. Y.; Song, J. S.; Shin, S. H.; Kim, S. J., *Smart Mat. Struct.* **2006,** 15, S74-S80.
32. Kittaka, S.; K., M.; Takahara, S., *J. Solid State Chem.* **1997,** 132, 447-450.
33. Yoshitake, H.; Abe, D., *Microporous Mesoporous Mater.* **2009,** 119, 267-275.
34. Edwards, H. G. M.; Russell, N. C., *J. Molec. Struct.* **1998,** 443, 223 - 231.
35. Ishioka, T.; Shibata, Y.; Takahashi, M.; Kanesaka, I.; Kitagawa, Y.; Nakamura, K. T., *Spectrochimica Acta Part A* **1998,** 54, 1827 - 1836.
36. Kanade, K. G.; Kale, B. B.; Aiyer, R. C.; Das, B. K., *Mater. Res. Bull.* **2006,** 41, 590 - 600.
37. Natarajan, S., *Solid State Sci.* **2002,** 4, 1331 - 1342.
38. Vaidhyanathan, R.; Natarajan, S.; Rao, C. N. R., *J. Chem. Soc., Dalton Trans.* **2001**, 699 - 706.
39. D'Antonio, M. C.; Mancilla, N.; Wladimirsky, A.; Palacios, D.; Gonzalez-Baro, A. C.; Baran, E. J., *Vib. Spec.* **2010,** Article in press.
40. Lagier, J. P.; Pezerat, H.; Dubernat, J., *Rev. Chim. Miner.* **1969,** 6, 1081 - 1093.
41. Bradley, D. C.; Mehrotra, R. C.; Gaur, D. P., *Metal Alkoxides*. Academic Press: London, 1978.
42. Brinker, C. J.; Scherer, G. W., *The Physics and Chemistry of Sol-Gel Science*. Academic Press: New York, 1990.
43. Nguyen, T.-V.; Choi, D.-J.; Yang, O.-B., *Res. Chem. Intermed.* **2005,** 31, 483-491.
44. Nolan, N. T.; Seery, M. K.; Pillai, S. C., *J. Phys. Chem. C* **2009,** 113, 16151 - 16157.
45. Phule, P. P.; Risbud, S. H., *J. Mater. Sci.* **1990,** 25, 1169-1183.
46. Doeuff, S.; Henry, M.; Sanchez, C.; Livage, J., **1987,** 89.
47. Mehrotra, R. C.; Bohra, R., *Metal Carboxylates*. Academic Press: London, 1983.
48. Yoldas, B. E., *Amer. Ceram. Soc. Bull.* **1975,** 54.
49. Livage, J.; Sanchez, C.; Henry, M.; Doeuff, S., *Solid State Ionics* **1989,** 32/33, 633-638.
50. Sugiura, M.; Ikeda, K., *J. Jpn. Ceram. Assoc.* **1947,** 55, 62 - 66.
51. Kim, H. T.; Kim, S. H.; Nahm, S.; Byun, J. D.; Kim, Y., *J. Am. Ceram. Soc.* **1999,** 82, 3043 - 3048.